Applied Physics Letters

Axially overlapped multi-focus light sheet with enlarged field of view

Cite as: Appl. Phys. Lett. **118**, 223701 (2021); https://doi.org/10.1063/5.0049013
Submitted: 28 February 2021 • Accepted: 30 April 2021 • Published Online: 02 June 2021

Hongjin Li, Zihan Wu, Zhichao Yang, et al.

Applied Physics Letters ARTICLE scitation.org/journal/apl

Axially overlapped multi-focus light sheet with enlarged field of view

Cite as: Appl. Phys. Lett. **118**, 223701 (2021); doi: 10.1063/5.0049013
Submitted: 28 February 2021 · Accepted: 30 April 2021 ·
Published Online: 2 June 2021

Hongjin Li,[1,2] Zihan Wu,[1] Zhichao Yang,[1,2] Karl Zhanghao,[1,a)] Peng Xi,[1,3] and Dayong Jin[1,2]

AFFILIATIONS

[1]UTS-SUSTech Joint Research Centre for Biomedical Materials and Devices, Department of Biomedical Engineering, College of Engineering, Southern University of Science and Technology, Shenzhen, Guangdong 518055, China
[2]Institute for Biomedical Materials and Devices (IBMD), Faculty of Science, University of Technology Sydney, NSW 2007, Australia
[3]Department of Biomedical Engineering, College of Future Technology, Peking University, Beijing 100871, China

[a)]**Author to whom correspondence should be addressed:** karl.hao.zhang@gmail.com

ABSTRACT

Light sheet fluorescence microscopy provides optical sectioning and is widely used in volumetric imaging of large specimens. However, the axial resolution and the lateral Field of View (FoV) of the system, defined by the light sheet, typically limit each other due to the spatial band product of the excitation objective. Here, we develop a simple multi-focus scheme to extend the FoV, where a Gaussian light sheet can be focused at three or more consecutive positions. Axially overlapped multiple light sheets significantly enlarge the FoV with improved uniformity and negligible loss in axial resolution. By measuring the point spread function of fluorescent beads, we demonstrated that the obtained light sheet has a FoV of 450 μm and a maximum axial FWHM of 7.5 μm. Compared with the conventional single-focus one, the multi-focus Gaussian light sheet displays a significantly improved optical sectioning ability over the full FoV when imaging cells and zebrafish.

Light sheet fluorescence microscopy (LSFM) has become an indispensable tool in volumetric imaging, with the advances in high spatiotemporal resolution and low photo-toxicity to the fluorescent sample. The open-source design with detailed instructions encourages DIY setups, which has significantly accelerated the wide-range adoption and applications of LSFM. Pioneering works, including OpenSPIM,[1] OpenSpin,[2] and the recent mesoSPIM,[3] provide detailed protocols for building and using the microscopes. These joint efforts further allow the biology labs to build their LSFM system for a specific application, including more complex schemes, such as multiview excitation or detection configurations.[4–6]

The key of LSFM is to generate a thin light sheet with a large field of view (FoV). The use of an illumination objective with a higher N.A. will generate a thinner light sheet, better for improving the axial resolution, as well as protecting the specimen from photobleaching due to the reduced illumination thickness. However, this is at the price of a smaller FoV. To solve this conflict between the axial resolution and FoV, the community has proposed various approaches.

The self-reconstructing beams, such as Bessel beams,[7,8] Airy beams,[9] and attenuation-compensated propagation-invariant beams,[10] have been used to maintain the thin sheet over a long propagation distance. Despite their superiority over Gaussian, these beams bring more sidelobes and photobleaching. To minimize the sidelobes, the combinations of light sheet illumination and confocal detection,[11,12] multi-photon excitation,[13–15] field modulation,[16] phase filters,[17] coherent,[18–20] and incoherent [21,22] superpositions have been proposed. Significantly, the dithered lattice light sheet has attracted much attention due to its high resolution and minimal photobleaching.[18] However, there are still different opinions doubting the superiority of self-reconstructing beams over Gaussian beams in light sheet microscopy.[23,24] Besides, the trade-off between N.A. and FoV seems to be the bottleneck for large-scale volumetric imaging with high resolution.

The other approach is to generate the light sheet with multiple beams. For example, the mSPIM[25] or SiMView[4] applied the dual-objective excitation configuration to double the FoV with similar axial resolution. Successive focus can be generated by axial scanning with tunable acoustic gradient-index (TAG)[26,27] lens, electrically tunable lens (ETL),[28,29] spatial light modulator (SLM),[30,31] multi-configuration,[32] and remote focusing optics.[33,34] Synchronization with a rolling shutter further increases the axial resolution.[33] However, during the process of creating the virtual thin light sheet, the actual exposure time in the focus region (Rayleigh region) is limited, and the specimen

beyond the in-focus area suffers from unnecessary photodamage. In a recent effort of the tiled light sheet, thin and small light sheet illumination was spliced to form a large FoV by focus shifting and sequential image acquisition at consecutive positions.[30] Furthermore, Yao *et al.* utilized SLM to generate multiple Gaussian beams simultaneously, instead of tiling the small light sheet from one position to another.[35] However, all these approaches require precise synchronization, which significantly increases the imaging system's complexity.

Inspired by the remote focusing mechanism,[36,37] here, we design an axially overlapped multi-focus system to break the trade-off between resolution and FoV, obtaining a high-resolution LSFM with extended FoV. Only one simple component is required: a multi-layer beam splitter (MBS), to generate multiple focal planes at different focal distances. The overlapped light sheets extend the FoV for over an order-of-magnitude, leading to high-resolution LSFM imaging at homogeneous illumination and sharp optical sectioning capability at a large scale. The easy implementation of the MBS makes our LSFM system low-cost, compact, and largely compatible with other LSFM systems. Following the open-source culture, we demonstrate the MF modular design on OpenSPIM, one of the most widely used light sheet systems.

The axially overlapped multi-focus light sheet (MF-LS) setup integrated into the OpenSPIM system is shown in Fig. 1. The axially overlapped MF-LS can be achieved with one polarization beam splitter (PBS), one quarter-wave plate (QWP), and MBS. The beam before PBS is horizontally polarized. After passing the PBS and 45° placed QWP, the rays reflected by MBS go through QWP with polarization changed to vertical and then be reflected by PBS to lens L2 and then the objective. The MBS consists of several beam-splitters and one mirror (Fig. S1), which produces consecutive beams with different divergence, resulting in multiple focusing on the illumination plane. Spacers with variable thickness can adjust the focus shift between neighboring beams, which is proportional to the distance between reflective layers by the ratio of the square of the magnification. Both the reflectivity of each beam splitter and the distance between neighboring reflectors should be well designed to generate the appropriate light sheet (Supplementary Note 1). This work focuses on the MBS setup with two beam splitters, which produces three primary foci.

We first conduct theoretical simulations to study the design and performance of the MBS. Generally, the FoV of a single Gaussian beam light sheet is considered to be twice the Rayleigh length (x_r)

$$FoV = 2x_r = 2\frac{\pi w_0^2}{\lambda}, \tag{1}$$

where the beam waist $w_0 = n\lambda/(\pi \text{N.A.})$ in a first approximation,[38] λ is the wavelength of the illumination beam, N.A. is the effective numerical aperture of illumination objective, and n is the refraction index.

We use N.A. = 0.064 in the simulation, which is consistent with our experimental setting. This N.A. results in a Rayleigh length of ~65 μm. Conveniently, the focus shift in the multi-focus beams is set to around the FoV or $2x_r$ of the Gaussian beam (supplementary material note 2). Besides, in our experiments, the axial shift between neighboring beams is much larger than the coherence length of the laser source. Therefore, the intensity profile of multiple shifted beams would be the sum of each beam under incoherent conditions [supplementary material note 3 and Eq. (S8)].

Figure 2(a) shows the intensity profiles, and Fig. 2(b) analyzes the FWHM distribution of the simulated beams under the single-, multi-, and swept focus mode with the same N.A. In the conventional single Gaussian beam, the axial resolution degrades rapidly beyond the Rayleigh region (N.A. = 0.064, x_r = 65 μm), resulting in a typical FoV of 220 μm with axial resolution better than 5.5 μm, which is the maximum FWHM within the Rayleigh region of triple-focus LS. MF-LS maintains the axial resolution over an enlarged FoV and shows significant improvements in uniformity. Double-focus light sheet can extend the effective FoV to ~380 μm. Triple-focus light sheet further increases the effective FoV to ~570 μm, enlarging the FoV by 2.6 times. Meanwhile, the performance of the MF mode is comparable to

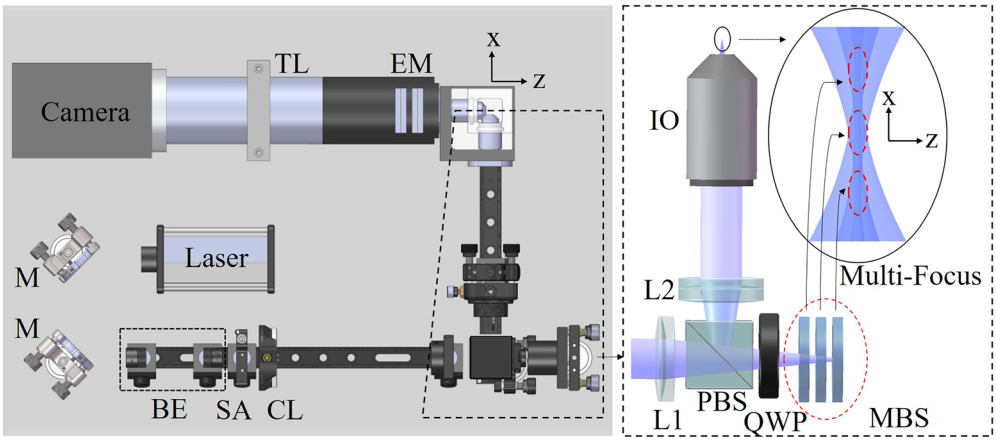

FIG. 1. Schematics of axially overlapped multi-focus light sheet (MF-LS) microscopy. The illumination beam from the laser source (473 nm, bandwidth 0.2 nm, MBL-III-473, CNI) passes through a 3× beam expander, a slit aperture (SA), a cylindrical lens (CL, ACY254-50-A, Thorlabs) and then is guided into the MF component. Finally, three foci are generated after the illumination objective (IO, Olympus, 10×/N.A. 0.3 W). The detailed information of the MF component is illustrated in the right part. It includes one polarization beam splitter (PBS, CCM1-PBS251, Thorlabs), a quarter-wave plate (QWP, WPA4420-450–650, Union Optics), and the multi-layer beam splitter (MBS), laid between a pair of lenses (L1, AC254-50-A and L2, AC254-150-A, Thorlabs). The detection path, which is composed of one detection objective (Olympus, 40×/N.A. 0.8 W), one emission filter (550LP, Thorlabs), the tube lens (Olympus, 0.5×), and the detector (Hamamatsu ORCA-Flash 4.0), is in the orthogonal direction with a total magnification of 20×.

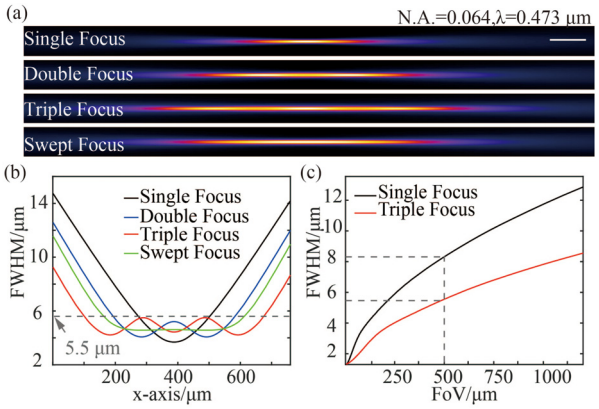

FIG. 2. Principle of axially overlapped MF-LS. (a) simulated image of the illumination beam for single-focus LS, MF-LS, and swept focus LS with the same N.A. (N.A. = 0.064). For MF-LS, the same Gaussian beams are focus shifted with doubled Rayleigh lengths (∼130 μm). Scale bar: 50 μm. (b) FWHM of the simulated light sheet at different positions along the illumination axis with N.A. = 0.064. (c) Both the FoV and FWHM change with the illumination N.A. The diagram shows the triple-focus LS has a much larger effective FoV than the single-focus LS.

the swept focus mode, showing more advantages at the edge of a larger FoV. Furthermore, we compared the average resolution within the Rayleigh regions between single-focus LS and triple-focus LS in Fig. 2(c). When requiring an effective FoV of 500 μm, the average resolution maintains at 5.5 μm in the triple-focus mode, while it falls to 8.3 μm in the single-focus mode.

Contrast, as the basis for resolution, is also an essential parameter in imaging. We compare contrast performance between the multi-focus light sheet and single-focus one by calculating the power ratio within FWHM of single Gaussian beam focus. The triple-focus light sheet shows an enhanced contrast over a larger FoV, while its contrast degrades to ∼80% of that of single Gaussian beam in the center area (supplementary material note 4).

The simulation assumes that multiple Gaussian beams are of the same intensity. To experimentally achieve a uniform light sheet, the reflectivity of each beam splitter should be well designed. With calculation, the optimum reflectivity of two beam splitters should be 23.5% and 39.5% for three foci (supplementary material Note 1). To reduce the cost, we use off-the-shelf beam-splitters with reflectivity of 27% and 40%. Besides the primary focus spots, there also exist some weaker focus spots due to multiple reflected beams, which can also be observed in experimental results. The detection path was set with a magnification of 20× with imaged FoV in terms of the camera sensor area, resulting in a maximum imaging area of 665×665 μm^2. The effective illumination N.A. was set to be around 0.064 in the experiments by adjusting the slit aperture (SA) shown in the schematics (Fig. 1). In the MBS, the thickness of spacers is set to be 2 mm, and the thickness of the beam splitters is 3 mm, resulting in the focus shift of ∼160 μm, slightly larger than the doubled Rayleigh lengths.

To experimentally implement our MF-LS scheme, first, we imaged the beam profile with scattered light in the single-focus mode [Fig. 3(a)] and triple-focus mode [Fig. 3(c)], respectively. The cylindrical lens (CL) shown in Fig. 1 was temporarily removed, and the SA is replaced with a circular aperture to adjust the effective illumination

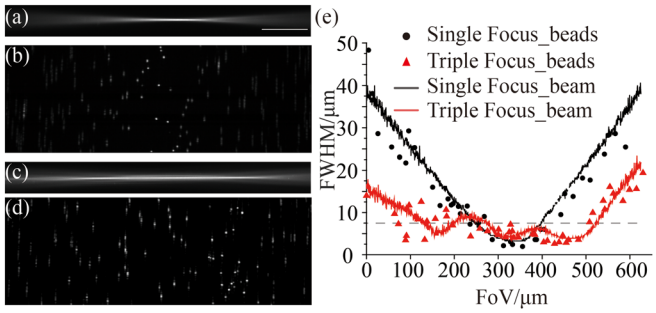

FIG. 3. Experimental measurements of the single-focus LS and triple-focus LS. (a) Profile of line beam imaged in single-focus mode and (c) in triple-focus mode over propagation (from left) length of 665 μm. The focus shift in the triple-focus LS is around 160 μm. (b) Maximum intensity projection (M. I. P) of microspheres (500 nm) embedded in 2% agarose in the x-z plane under single- and (d) under triple-focus LS illumination. Scale bar: 100 μm. (e) Comparison of the FWHM of the images of the line beam with scattering light (line-plot) and the axial FWHM of fluorescent images of microspheres (dot-plot) over the FoV.

N.A. In the single-focus scheme, the laser power was ∼1.9 mW in the pupil plane and increased to ∼5.4 mW in the triple-focus mode with an exposure time of 15 ms. From the FWHM distributions of the measured beams [Fig. 3(e)], it can be seen that, though the single-focus light sheet achieved a higher resolution at the center (∼3 μm), the resolution dropped rapidly when the FoV became larger, e.g., ∼7.5 μm at the FoV of ∼150 μm in diameter. In contrast, in the triple-focus light sheet, the FoV could be extended to approximately ∼400 μm in diameter with a consistent resolution better than 7.5 μm. Within the FoV of ∼400 μm, the triple-focus light sheet shows a more uniform performance in contrast. However, similar to the simulation results, the triple-focus light sheet has worse contrast in the center area due to the more side lodes from other focused beams. Besides, the MF-LS uses more than two times excitation power in the experiments, which will cause some extra photobleaching (supplementary material note 4).

The calibration experiments with fluorescent microspheres (500 nm) fixed in 2% agarose were carried out under single-focus vs triple-focus illumination, respectively. In the calibration experiment, we changed the detection objective with a low N.A. one (Olympus, 10×/N.A. 0.3 W), in which the axial resolution is determined by the thickness of the light sheet. Figure 3(b) shows the Maximum Intensity Projection (M. I. P.) image of the fluorescent beads under single-focus LS illumination, and Fig. 3(d) shows that under triple-focus LS. The single-focus LS covers a FoV of ∼150 μm in diameter with axial resolution beyond 7.5 μm. In contrast, the triple-focus LS covers an FoV of ∼450 μm, consistent with line beam imaging analysis [Fig. 3(e)].

Furthermore, we evaluated the performance of MF-LS on different biological specimens. For single-focus light sheet illumination, the laser power was set to ∼0.06 mW with an exposure time of 25 ms and then turned up to ∼0.18 mW in the triple-focus mode. Hela cells and juvenile zebrafish were fixed in 2% agarose inside a glass capillary (1 mm diameter) and then pushed out for imaging. Nile red labeled Hela cells were imaged with the single-focus LS and the triple-focus LS. The triple-focus illumination showed better illumination uniformity in the x–y perspective [Figs. 4(a) and 4(b)]. In the x–z perspective, the cells on the border appear to be elongated and blurred in the single-focus image [Fig. 4(c)] due to increased FWHM of the light

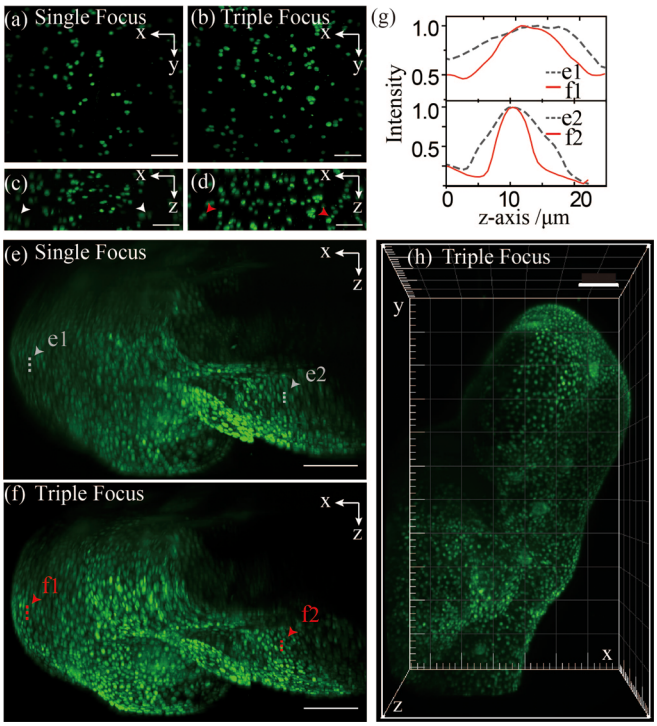

FIG. 4. Experimental data with biological specimens for single-focus and triple-focus LS. (a–d) M. I. P images of Hela cells labeled by Nile red for single-focus and triple-focus LS in the x–y plane (a) and (b) and x–z plane (c) and (d). (e) and (f) M. I. P of fixed juvenile zebrafish labeled SYTOX™ Green Nucleic Acid Stain in the x-z plane ($\Delta x \times \Delta z = 665 \times 460\ \mu m^2$) for single-focus LS (e) and triple-focus LS (f). (g) The line profiles of nucleus show better optical sectioning and axial resolution of the triple-focus LS than the single-focus LS. (h) 3D volumetric view ($\Delta x \times \Delta y \times \Delta z = 665 \times 1100 \times 460\ \mu m^3$) of the zebrafish illuminated by MF-LS. Scale bar: 100 μm.

sheet, while those cells are still in round shape in the triple-focus images [Fig. 4(d)]. These observations are consistent with the quantitative imaging results with the fluorescent microspheres. Afterward, fixed ~3-day-old juvenile zebrafish were labeled with SYTOX™ Green Nucleic Acid Stain and imaged. As shown in the x-z M. I. P image in single-focus LS [Fig. 4(e)], and triple-focus LS [Fig. 4(f)], the shape of cells was elongated along the z-axis on the border in single-focus LS, showing a larger FWHM than that in triple-focus LS [Fig. 4(g)]. Besides, the fluorescent intensity on the border area drops to only 25% of that in the center area in single-focus. In contrast, the fluorescent intensity on the border area remains 50% of that in the center area in triple-focus LS.

In summary, we propose an axially overlapped multi-focus scheme to break the trade-off between resolution and FoV of the light sheet. We demonstrate the triple-focus Gaussian light sheet with theoretical simulation and experimental imaging results, exhibiting almost one-order-of-magnitude higher imaging area. The performance of the three-focus light sheet is superior to that of dual-objective excitation with a more simplified system and much lower cost. Moreover, the MF setup is compatible with the dual-objective excitation, which can further extend the effective FoV and make the illumination more uniform when one side of the specimen is heavily scattering. Compared with the tiled light sheet,[30] the whole FoV is imaged with only one acquisition so that the imaging speed is not sacrificed.

We anticipate that the axial overlapped MF scheme also applies to four or more foci and multiple excitation objectives. It should be noted that to generate multiple foci, the laser power needs to be increased correspondingly, and it may become harder to keep the parallelism among reflective layers. Thus, precise manufacturing of multiple reflective layers would be necessary. The MF-LS is demonstrated with a medium axial resolution of micrometers by relatively low N.A. illumination so that the optical aberration is not severe. Obtaining high resolution with high illumination N.A. at large FoV requires not only optical aberration optimization[36,37] but also precise manufacturing of the MBS. Besides, the coherent interference effect may become a problem with reduced foci shift (supplementary material Note 3). In these applications, the scheme of remote focusing is preferred currently despite the more complicated system and higher cost. Our MF-LS setups are cost-effective, versatile, and can be integrated into many existing light sheet systems with minimum effort. Therefore, our design can upgrade existing light sheet systems that aim at imaging large FoV at cellular resolution.

See the supplementary material for supporting content.

This work was supported by the National Natural Science Foundation of China (Nos. 62005116, 61729501, and 51720105015) and the Science and Technology Innovation Commission of Shenzhen (No. KQTD20170810110913065 and RCBS20200714114817138).

DATA AVAILABILITY

The data that support the findings of this study are available from the corresponding author upon reasonable request.

REFERENCES

[1]P. G. Pitrone, J. Schindelin, L. Stuyvenberg, S. Preibisch, M. Weber, K. W. Eliceiri, J. Huisken, and P. Tomancak, Nat. Methods **10**(7), 598–599 (2013).
[2]E. J. Gualda, T. Vale, P. Almada, J. A. Feijo, G. G. Martins, and N. Moreno, Nat. Methods **10**(7), 599–600 (2013).
[3]F. F. Voigt, D. Kirschenbaum, E. Platonova, S. Pages, R. A. A. Campbell, R. Kastli, M. Schaettin, L. Egolf, A. van der Bourg, P. Bethge, K. Haenraets, N. Frezel, T. Topilko, P. Perin, D. Hillier, S. Hildebrand, A. Schueth, A. Roebroeck, B. Roska, E. T. Stoeckli, R. Pizzala, N. Renier, H. U. Zeilhofer, T. Karayannis, U. Ziegler, L. Batti, A. Holtmaat, C. Luscher, A. Aguzzi, and F. Helmchen, Nat. Methods **16**(11), 1105–1108 (2019).
[4]R. Tomer, K. Khairy, F. Amat, and P. J. Keller, Nat. Methods **9**(7), 755–763 (2012).
[5]Y. Wu, P. Wawrzusin, J. Senseney, R. S. Fischer, R. Christensen, A. Santella, A. G. York, P. W. Winter, C. M. Waterman, Z. Bao, D. A. Colon-Ramos, M. McAuliffe, and H. Shroff, Nat. Biotechnol. **31**(11), 1032–1038 (2013).
[6]R. K. Chhetri, F. Amat, Y. Wan, B. Hockendorf, W. C. Lemon, and P. J. Keller, Nat. Methods **12**(12), 1171–1178 (2015).
[7]F. O. Fahrbach and A. Rohrbach, Opt. Express **18**(23), 24229–24244 (2010).
[8]F. O. Fahrbach, P. Simon, and A. Rohrbach, Nat. Photonics **4**(11), 780–785 (2010).
[9]T. Vettenburg, H. I. Dalgarno, J. Nylk, C. Coll-Llado, D. E. Ferrier, T. Cizmar, F. J. Gunn-Moore, and K. Dholakia, Nat. Methods **11**(5), 541–544 (2014).
[10]J. Nylk, K. McCluskey, M. A. Preciado, M. Mazilu, Z. Yang, F. J. Gunn-Moore, S. Aggarwal, J. A. Tello, D. E. K. Ferrier, and K. Dholakia, Sci. Adv. **4**(4), eaar4817 (2018).
[11]F. O. Fahrbach and A. Rohrbach, Nat. Commun. **3**, 632 (2012).
[12]E. Baumgart and U. Kubitscheck, Opt. Express **20**(19), 21805–21814 (2012).

[13]S. C. Lau, H. C. Chiu, L. Zhao, T. Zhao, M. M. T. Loy, and S. Du, Rev. Sci. Instrum. **89**(4), 043701 (2018).
[14]N. A. Hosny, J. A. Seyforth, G. Spickermann, T. J. Mitchell, P. Almada, R. Chesters, S. J. Mitchell, G. Chennell, A. C. Vernon, K. Cho, D. P. Srivastava, R. Forster, and T. Vettenburg, Biomed. Opt. Express **11**(7), 3927–3935 (2020).
[15]F. O. Fahrbach, V. Gurchenkov, K. Alessandri, P. Nassoy, and A. Rohrbach, Opt. Express **21**(11), 13824–13839 (2013).
[16]X. Xu, J. Chen, B. Zhang, L. Huang, Y. Zheng, K. Si, S. Duan, and W. Gong, Opt. Lett. **45**(17), 4851–4854 (2020).
[17]S. Ryu, B. Seong, C. W. Lee, M. Y. Ahn, W. T. Kim, K. M. Choe, and C. Joo, Biomed. Opt. Express **11**(7), 3936–3951 (2020).
[18]B. C. Chen, W. R. Legant, K. Wang, L. Shao, D. E. Milkie, M. W. Davidson, C. Janetopoulos, X. S. Wu, J. A. Hammer III, Z. Liu, B. P. English, Y. Mimori-Kiyosue, D. P. Romero, A. T. Ritter, J. Lippincott-Schwartz, L. Fritz-Laylin, R. D. Mullins, D. M. Mitchell, J. N. Bembenek, A. C. Reymann, R. Bohme, S. W. Grill, J. T. Wang, G. Seydoux, U. S. Tulu, D. P. Kiehart, and E. Betzig, Science **346**(6208), 1257998 (2014).
[19]T. A. Planchon, L. Gao, D. E. Milkie, M. W. Davidson, J. A. Galbraith, C. G. Galbraith, and E. Betzig, Nat. Methods **8**(5), 417–423 (2011).
[20]L. V. Nhu, X. Hoang, M. Pham, and H. Le, Eur. Phys. J. Plus **135**(6), 426 (2020).
[21]B. J. Chang, M. Kittisopikul, K. M. Dean, P. Roudot, E. S. Welf, and R. Fiolka, Nat. Methods **16**(3), 235–238 (2019).
[22]L. Gao, L. Shao, C. D. Higgins, J. S. Poulton, M. Peifer, M. W. Davidson, X. Wu, B. Goldstein, and E. Betzig, Cell **151**(6), 1370–1385 (2012).
[23]B. J. Chang, K. M. Dean, and R. Fiolka, Opt. Express **28**(18), 27052–27077 (2020).
[24]E. Remacha, L. Friedrich, J. Vermot, and F. O. Fahrbach, Biomed. Opt. Express **11**(1), 8–26 (2020).
[25]J. Huisken and D. Y. Stainier, Opt. Lett. **32**(17), 2608–2610 (2007).
[26]W. Zong, J. Zhao, X. Chen, Y. Lin, H. Ren, Y. Zhang, M. Fan, Z. Zhou, H. Cheng, Y. Sun, and L. Chen, Cell Res. **25**(2), 254–257 (2015).
[27]K. M. Dean and R. Fiolka, Opt. Express **22**(21), 26141–26152 (2014).
[28]F. O. Fahrbach, F. F. Voigt, B. Schmid, F. Helmchen, and J. Huisken, Opt. Express **21**(18), 21010–21026 (2013).
[29]P. N. Hedde and E. Gratton, Microsc. Res. Tech. **81**(9), 924–928 (2018).
[30]L. Gao, Opt. Express **23**(5), 6102–6111 (2015).
[31]L. Gao, W. C. Tang, Y. C. Tsai, and B. C. Chen, Opt. Express **27**(2), 1497–1506 (2019).
[32]K. M. Dean, P. Roudot, E. S. Welf, T. Pohlkamp, G. Garrelts, J. Herz, and R. Fiolka, Optica **4**(2), 263–271 (2017).
[33]K. M. Dean, P. Roudot, E. S. Welf, G. Danuser, and R. Fiolka, Biophys. J. **108**(12), 2807–2815 (2015).
[34]S. Deng, Z. Ding, D. Yuan, M. Liu, and H. Zhou, J. Opt. Soc. Am. A **38**(1), 19–24 (2021).
[35]C. Liu, C. Bai, X. Yu, S. Yan, Y. Zhou, X. Li, J. Min, Y. Yang, D. Dan, and B. Yao, Opt. Express **29**(4), 6158–6168 (2021).
[36]E. J. Botcherby, R. Juskaitis, M. J. Booth, and T. Wilson, Opt. Lett. **32**(14), 2007–2009 (2007).
[37]E. J. Botcherby, R. Juskaitis, M. J. Booth, and T. Wilson, Opt. Commun. **281**(4), 880–887 (2008).
[38]O. E. Olarte, J. Andilla, E. J. Gualda, and P. Loza-Alvarez, Adv. Opt. Photonics **10**(1), 111–179 (2018).